Discrete and continuous invariance in phyllotactic tilings

Patrick D. Shipman*
Department of Mathematics, Colorado State University, 1874 Campus Delivery, Fort Collins, Colorado 80523-1874, USA
(Received 7 December 2009; published 5 March 2010)

Phyllotaxis refers to the arrangement of primordia (the first stage in the development of a structure such as a leaf) on plants and *phyllotactic planforms* refer to the shapes of the primordia in a phyllotactic arrangement. This paper focuses on invariances in phyllotactic planforms as the van Iterson parameter Γ—a measurement of the ratio of the size of the annular generative region at the plant tip where the patterns form to primordium area—varies. We demonstrate *discrete invariance* in phyllotactic planforms, by which we mean a similarity in the planform under a scaling $\Gamma \to \Gamma\phi^n$, where ϕ is the golden number and n is an integer. *Continuous invariance* in planforms is then motivated by examples in which the shapes of primordia are homogeneous as n varies over the real numbers. We also show how continuous invariance results from classical number-theoretical theorems on the approximation of irrational numbers (such as ϕ) by rational numbers. We define these notions first for the underlying phyllotactic lattice and then for primordium shapes and amplitude equations resulting from partial differential equation (PDE) models.

DOI: 10.1103/PhysRevE.81.031905 PACS number(s): 87.10.−e, 87.19.lp, 87.19.lx, 02.30.Jr

I. INTRODUCTION

Inspecting a sunflower head such as one of those in Fig. 1, one may notice first the diamond-shaped seeds that tile the disk. Families of spirals catch the eye, and if one counts the numbers of spirals in each family, one typically arrives at successive members of the Fibonacci sequence $1,1,2,3,\ldots$ or another Fibonacci-like sequence. The spiral families seem to blend into each other so that lower members of the sequence are observed near the center of the disk and higher numbers as one works one's way out. But one notices that the seeds in the sunflower in Fig. 1 remain the same diamond shape even as the observed number of spirals varies.

Phyllotaxis refers to the arrangement of elements such as leaves, seeds, and florets at plant meristems. The arrangement of the sunflower seeds in Fibonacci spirals is one example; another commonly observed phyllotactic arrangement is the *decussate* phyllotaxis in which the elements alternate in pairs. By *phyllotactic planform* we refer to the shapes of the elements as well as their arrangement. The plant world provides us with planforms dominated by ridges, regular hexagons, and irregular hexagons, as well as diamonds. In this sense, these planforms provide examples of the universality of pattern formation in that polygonal planforms are observed in many natural and laboratory (e.g., Raleigh-Bènard convection) systems governed by nonlinear equations [6]. In [23,25,38,39], we describe the relationship between phyllotaxis and phyllotactic planforms and analyze partial differential equation (PDE) models for the formation of these planforms based on biomechanical and chemical mechanisms. In particular, we show how quadratic nonlinearities in the governing equations give rise to planforms dominated by triads of Fourier modes with wave vectors $\vec{k}$ satisfying a Fibonacci-like condition $\vec{k}_1+\vec{k}_2=\vec{k}_3$.

Fibonacci-like sequences are not, however, generally observed in pattern-forming systems. The geometry of the process whereby phyllotactic patterns form is unique. *Primordia*, the initial bumps that mature into elements such as leaves or seeds, originate in an annular *generative region* surrounding the tip of a growing plant apex. The primordia then grow in size and develop in shape as they move away from the plant tip (due to growth of the apex away from them). But, the angular positions of the primordia typically remain unchanged in this process, so that their relative positions change only in radial spacing. The process of primordium initiation and development occurs on a plant apex with a geometry that varies from a cylinder to a hemisphere to being relatively flat [21]. While some investigations of phyllotaxis (notably those of Bravais and Bravais [2] and van Iterson [41]) have been expressed as lattices on cylinders, others (such as Church [3] and Richards [33]) have worked in planar annuli. In the case of a cylinder, the crucial parameter is the radius R, which, in the spherical geometry, can be interpreted as the distance that the primodia form from the very tip of the plant apex.

A key quantity used to describe phyllotactic patterns is the ratio of R to the (typically thought of as constant) size S of

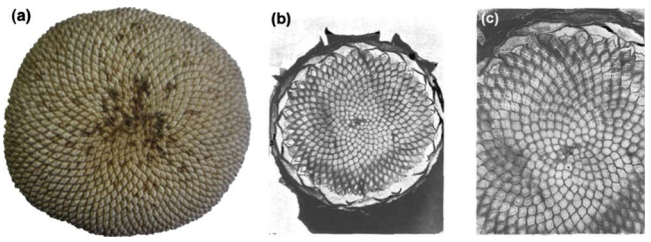

FIG. 1. (Color online) Sunflower seed heads. (a) The spiral families come in Fibonacci numbers in this sunflower seed head. (b) and (c) A seed head of *helianthus annuus*, reproduced from Church's *On the Relation of Phyllotaxis to Mechanical Laws* [3]. Church referred to this as an *anomalous capitulum* as the spiral families come in the Fibonacci-like sequence $\ldots,11,18,29,47,\ldots$ rather than the (classical) Fibonacci sequence. Some of the spirals are marked in (c); note the transition from one family of spirals marked in white to the next.

*shipman@math.colostate.edu

newly formed primordia. This ratio takes various forms depending on how primordium size is measured, but it may generally be referred to as the van Iterson parameter. van Iterson himself represented primordia as disks, so that S would be the diameter of a disk, and this approach has figured in the work of many authors since [1,9,10]. In an experimental paradigm simulating primordium formation using repelling magnetic droplets, Douady and Couder were able to produce Fibonacci-spiral patterns and transitions up the Fibonacci sequence by continuously increasing the van Iterson parameter, which we shall call Γ. (Like van Iterson, these authors use a parameter analogous to the inverse of Γ as defined in this paper, so that they decrease Γ to move up the Fibonacci sequence.) Douady and Couder also reproduced in their experiment the *van Iterson diagram*, which relates Γ to observed divergence angles $2\pi d$ of the phyllotactic pattern. The divergence angle, as explained in Sec. II A, is the angle around the plant apex between consecutively formed primordia. The value of d associated with Fibonacci-spiral patterns is commonly observed to be approximately $d=1-1/\phi_+$, where $\phi_+=\frac{1+\sqrt{5}}{2}$ is the golden number, the positive root of $x^2-x-1=0$. Hotton [14] and Atela *et al.* [1] studied symmetries in the van Iterson diagram related to hyperbolic geometry and pointed out that for certain pairs (Γ,d) the phyllotactic tiling is hexagonal or square. Much has been written on phyllotaxis, the Fibonacci sequence and the golden number; useful overviews are given by Jean [18] and Jean and Barabé [19].

The purpose of this paper is to demonstrate number-theoretical and geometric relationships that come into play in the analysis of PDE models. The paper is organized into four sections. Section II focuses on phyllotactic lattices (phyllotaxis) as a preparation for the more general study of phyllotactic planforms and PDE models in Sec. III. We begin by reviewing properties of lattices defined on cylinders and the connection to phyllotaxis. We show how it is that the existence of an eigenvalue $-1/\phi_+$ for the Fibonacci Q matrix that defines Fibonacci-like sequences gives rise to an invariance in the lattice under a scaling $\Gamma\to\Gamma\phi_+$ of the van Iterson parameter. This we call *discrete invariance*. The key result of Sec. II is contained in Sec. II F. Section II F begins with a review of classical number-theoretical results on the approximation of irrational numbers by rational numbers through continued fraction expansions and then uses these results to calculate continuous curves (see Fig. 2) analogous to those sketched by Coxeter [5] on which the basis vectors for a phyllotactic lattice evolve as Γ changes. This we call *continuous invariance*. The connection with PDE models is contained in Sec. III, which is a full account of results sketched in [24]. In this section, we first review the analysis of our biomechanical and biochemical models for phyllotaxis, in which PDE models with strong quadratic nonlinearities are reduced to ordinary differential equation (ODEs) , solutions of which give the amplitudes and wave vectors of Fourier representations of the plant surface in the generative region [25–27,39]. Motivated by the work of Hotton and Atela *et al.*, we then show how, for values of Γ corresponding to rhombic tilings, symmetries aid in the solution of the equations for the amplitudes and wave vectors. The notions of discrete and continuous invariance are then extended to these solutions, thus demonstrating discrete and continuous invariance of phyllotactic planforms.

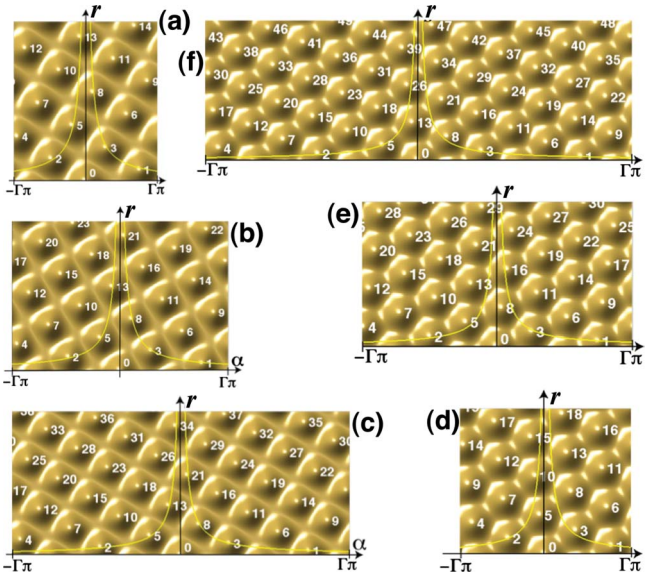

FIG. 2. (Color online) The maxima of the graphed $\mathbb{L}$-periodic functions (see Sec. III) correspond to cylindrical lattices $\mathbb{L}(A=1,\Gamma,d=1+\phi_-,g=1)$ for various values of Γ. For $\Gamma_S^2=3^2+5^2=34$, $\Gamma_H^2=\frac{2}{\sqrt{3}}(3^2+15+5^2)$, and $\phi_+=\frac{1+\sqrt{5}}{2}$, these values are (a) $\Gamma=\Gamma_S/\phi_+$, (b) $\Gamma=\Gamma_S$, (c) $\Gamma=\Gamma_S\phi_+$, (d) Γ_H/ϕ_+, (e) Γ_H, and (f) $\Gamma_H\phi_+$. In each graph, the horizontal axis is θ, given for the interval $\theta\in[-\Gamma\pi,\Gamma\pi]$, and the vertical axis is r. The points are numbered from smallest to largest r-coordinate value. Also plotted on each graph are the curves $\sqrt{A}(\frac{1}{\rho},\pm\frac{\rho}{\sqrt{5}})$ calculated in Sec. III D.

II. INVARIANCE OF CYLINDRICAL LATTICES

Phyllotactic patterns are typically approximated locally by lattices, and we begin in Sec. II A by reviewing the notation for lattices on cylinders and a basis matrix Ω, as presented in [38,39]. Rhombic lattices are discussed in Sec. II B, and Sec. II C translates these results to an annulus in the plane. In Sec. II D, Fibonacci-like sequences of basis matrices Ω_ν are studied to provide a new relationship between noble numbers and invariance as defined in Sec. II E. Classical number-theoretical results on the approximation of noble numbers by rational numbers motivate a proposition in Sec. II F on the limiting values of the entries of Ω_ν as ν increases, as well as a definition of continuous invariance.

A. Coordinates and bases

A Bravais lattice $\mathbb{L}$ in $\mathbb{R}^2$ consists of all integer combinations $z_1\vec{v}+z_2\vec{w}$ of vectors $\vec{v},\vec{w}\in\mathbb{R}^2$, $(z_1,z_2)\in\mathbb{Z}^2$. The lattice is periodic in $\vec{u}\in\mathbb{R}^2$ if $\vec{\omega}+\vec{u}\in\mathbb{L}$ for all $\vec{\omega}\in L$. Such a lattice can be rolled onto a cylinder of circumference $2\pi R=k\|\vec{u}\|$ for $k\in\mathbb{N}$. We will consider cylindrical lattices of the form

$$\mathbb{L}(\lambda,R,d,g)=\left\{z_1(\lambda,2\pi Rd)+z_2\left(0,\frac{2\pi R}{g}\right):(z_1,z_2)\in\mathbb{Z}^2\right\},$$

where $\lambda\in\mathbb{R}^+$, $g\in\mathbb{N}$, and $d\in[0,1]$. $\mathbb{L}$ can be thought of as a $(0,\frac{2\pi R}{g})$-periodic lattice in $\mathbb{R}^2$ or as a lattice on a cylinder of

radius R. In the following, we will use coordinates (r,α) for points in $\mathbb{R}^2$; α denotes a scaled angle in $(-\pi R,\pi R)$.

The vectors $\vec{\omega}_{\lambda,d}=(\lambda,2\pi Rd)$ and $\vec{\omega}_g=(0,\frac{2\pi R}{g})$ form one basis for $\mathbb{L}$. All other bases are found by taking the linear combinations

$$\begin{pmatrix}\alpha & \beta\\ \gamma & \delta\end{pmatrix}\begin{pmatrix}\lambda & 2\pi Rd\\ 0 & \dfrac{2\pi R}{g}\end{pmatrix}=\begin{pmatrix}\lambda\alpha & 2\pi\left(d\alpha+\dfrac{\beta}{g}\right)\\ \lambda\gamma & 2\pi\left(d\gamma+\dfrac{\delta}{g}\right)\end{pmatrix},$$

where $\alpha,\beta,\delta,\gamma\in\mathbb{Z}$ and $\alpha\delta-\beta\gamma=\pm 1$. Setting $m\doteq g\alpha$, $n\doteq g\gamma$, $p\doteq\delta$, and $q\doteq\beta$, this means that all bases of $\mathbb{L}(\lambda,R,d,g)$ are given by $\vec{\omega}_m,\vec{\omega}_n$, where $m,n\in\mathbb{Z}$, $pm-qn=\pm g=\pm\gcd(m,n)$, and

$$\Omega_{(m,n)}(\lambda,R,d,g)\doteq\begin{pmatrix}\vec{\omega}_n\\ \vec{\omega}_m\end{pmatrix}\doteq\frac{1}{g}\begin{pmatrix}\lambda n & 2\pi R(nd-p)\\ \lambda m & 2\pi R(md-q)\end{pmatrix}.$$

The matrix Ω depends on four parameters λ,R,d,g that determine the lattice $\mathbb{L}(\lambda,R,d,g)$ and four parameters m,n,p,q related by $pm-qn=\pm\gcd(m,n)=\pm g$ which choose a basis for $\mathbb{L}$.

For any choice of m,n and p,q such that $pm-nq=\pm g$, $(p+kn)m-(q+km)n=\pm g$ for any integer k. Thinking of $\mathbb{L}$ as a lattice on a cylinder $[0,\infty)\times(-\pi R,\pi R)$, an ideal choice of p,q is one for which

$$-\pi R<\frac{2\pi R}{g}(md-p),\quad \frac{2\pi R}{g}(nd-q)<\pi R.$$

Rewritting this condition shows that

$$\left|\frac{p}{m}-d\right|<\frac{g}{2m},\quad \left|\frac{q}{n}-d\right|<\frac{g}{2n}.$$

This says that both $\frac{p}{m}$ and $\frac{q}{n}$ should be good approximations of d. For arbitrary $m,n\in\mathbb{N}$ and d, it is not always possible to find p,q that satisfy these conditions. (Try, for example, $m=6$, $n=7$, $d=\frac{3}{8}$.) In Sec. II F, we show how classical theorems on the approximation of irrational numbers (such as an irrational choice of d) by rational numbers relate to special choices of m,n,p,q,d that allow for invariance in cylindrical lattices in the annular geometry as described in Sec. II C.

The area A associated with each point in the lattice $\mathbb{L}(\lambda,R,d,g)$ is defined to be the determinant of Ω,

$$A\doteq\det\Omega=2\pi R\frac{\lambda}{g}.$$

Solving this last expression for $\lambda=\frac{gA}{2\pi R}$, we can restate the matrix Ω as a function of A,R,d,g,

$$\Omega_{(m,n)}(A,R,d,g)=\begin{pmatrix}\dfrac{A}{2\pi R}n & \dfrac{2\pi R}{g}(nd-p)\\ \dfrac{A}{2\pi R}m & \dfrac{2\pi R}{g}(md-q)\end{pmatrix}.\qquad(1)$$

Another useful form for Ω results from defining $\Gamma\doteq\frac{2\pi R}{\sqrt{A}}$, so that

$$\Omega_{(m,n)}(A,\Gamma,d,g)=\sqrt{A}\begin{pmatrix}\dfrac{n}{\Gamma} & \dfrac{\Gamma}{g}(nd-p)\\ \dfrac{m}{\Gamma} & \dfrac{\Gamma}{g}(md-q)\end{pmatrix}.$$

The parameter Γ is our version of the van Iterson parameter. In the following, we will also write a cylindrical lattice as $\mathbb{L}=\mathbb{L}(A,\Gamma,d,g)$.

B. Rhombic cylindrical lattices

Although the parameter d observed on real plants is typically nearly constant over wide areas of the pattern, it does vary. van Iterson [41] (see also [8]) showed how d can be chosen as a function of a parameter analogous to Γ, so that, as Γ increases continuously, the lattice $\mathbb{L}(A,\Gamma,d,g)$ is always *rhombic*. In particular, square and hexagonal lattices are possible for certain choices of d and Γ. These values of Γ have been calculated by Hotton [14] and Douady [8]. In terms of the matrix notation used in this paper, the values are as follows:

(1) *Square lattices.* Solving $\Omega_{(m,n)}^T\Omega_{(m,n)}=AI$, where I is the identity matrix, for d and Γ, we find that $d=(qm+pn)/(m^2+n^2)$ and $\Gamma^2=m^2+n^2$.

(2) *Hexagonal lattices.* Solving $\|\vec{\omega}_m\|=\|\vec{\omega}_n\|=\|\vec{\omega}_m\vec{\omega}_n\|$ for Γ and d yields $d=[mp+nq+2(np+mq)]/[2(m^2+mn+n^2)]$ and $\Gamma^2=\frac{2}{\sqrt{3}}(m^2+mn+n^2)$.

Examples of square and hexagonal lattices are shown in Fig. 2. The surfaces plotted in this figure are explained in Sec. III, but the lattices currently under discussion correspond to the surface maxima. The lattice points are labeled according to increasing radial (vertical) coordinate, so that point 5, for example, is located at vector $\vec{\omega}_5$. Two observations motivate our subsequent discussion:

(1) As Γ is changed to $\Gamma\phi_+$, where $\phi_+=\frac{1+\sqrt{5}}{2}$ is the golden number, the lattice remains locally the same after a reflection about the vertical axis.

(2) For the square lattice in Figs. 2(a)–2(c), a Fibonacci-like sequence $\{\omega_\nu\}$ of lattice vectors $\omega_3,\omega_5,\omega_8=\omega_3+\omega_5,\ldots,\omega_{\nu+2}=\omega_\nu+\omega_{\nu+1}$ lies close to hyperbolic curves, so that the angular component of ω_ν approaches 0 as ν increases.

By transferring our study of cylindrical lattices to the annular geometry, we will obtain another motivation for the study of Fibonacci-like sequences of wave vectors $\{\omega_\nu\}$.

C. Cylindrical lattices in the annulus

The patterns that we observe sunflowers, for example, are topologically cylindrical (upon removal of the center point, which does not belong to any tile) but geometrically closer to annuli in the plane. These patterns display cylindrical lattices in that the positions of seeds or analogous elements (with radial distance measured in arclength along the curved region) are given by

$$\left[f(j)\cos\left(2\pi dj+\frac{2\pi}{g}k\right),f(j)\sin\left(2\pi dj+\frac{2\pi}{g}k\right)\right],$$

where $f(j)$ is typically approximately $f(j)=f_1(j)=\hat{\lambda}^j$ or $f(j)=f_2(j)=\sqrt{j\hat{\lambda}}$. The parameter d will depend on j, but in

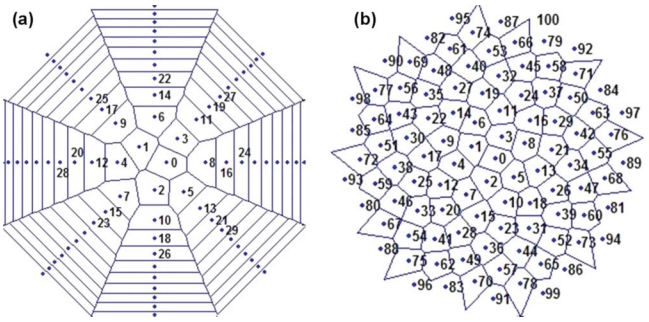

FIG. 3. (Color online) The image, under the transformation T, of the cylindrical lattices (a) $\mathbb{L}(A=1,\Gamma=1,d=\frac{3}{8},g=1)$ and (b) $\mathbb{L}[A=1,\Gamma=1,d=\frac{1}{2}(3-\sqrt{5}),g=1]$. The points are numbered according to their distance from the origin. Also plotted are the corresponding Voronoi polygons.

many cases it can be approximated by a constant and it typically approaches a constant for large j. The (r,α) coordinates of the seed centers are thus approximately a cylindrical lattice $\mathbb{L}(\lambda,R=1,d,g)$. Since many plants display the function $f_1(j)$, the parameter λ is typically called the plastochrone ratio.

For a pattern described by the function f_2, the seeds will be of equal area. To show this, let us translate our results on cylindrical lattices in the plane to the disk by finding an equiarial transformation from the plane to the disk. An equiarial transformation T is one for which the area of any set Σ of points in the domain is equal to the area of the image of Σ under T. Denoting the coordinates of the plane in which the cylindrical lattice $\mathbb{L}(\lambda,R=1,d,g)$ lies by (s,θ) [R is taken to be 1 so that the second coordinate can be considered as an angle in $(-\pi,\pi)$] and the coordinates of the plane in which the disk lies by (x,y), we seek a transformation of the form

$$(x,y)=T'(s,\theta)=[f(s)\cos\theta,f(s)\sin\theta],\quad s\geq 0,\theta\in(-\pi,\pi),$$

so that, in polar coordinates (r,α), points in the (x,y) plane are given by

$$(r,\alpha)=\tilde{T}'(s,\theta)=[f(s),\theta].$$

The Jacobian of T' is

$$J_{T'}=\begin{pmatrix} f'(s)\cos\theta & -f(s)\sin\theta \\ f'(s)\sin\theta & f(s)\cos\theta \end{pmatrix}$$

and $\det J_{T'}=f'(s)f(s)$. Solving the equation $f'(s)f(s)=A'$ for $f(s)$, where A' is a given constant, we find that $f(s)=\sqrt{2A's+s_0}$. Here, s_0 is the image under T' of the line $(s=0,\theta)$. The transformation

$$T(s,\theta)=(\sqrt{2A's+s_0}\cos\theta,\sqrt{2A's+s_0}\sin\theta) \tag{2}$$

is thus equiarial if $A'=1$.

Consider two examples of the image under Eq. (2) in the annulus of cylindrical lattices $\mathbb{L}$ in the (s,θ) plane, as suggested by Rothen and Koch [37]. The images of the lattices $\mathbb{L}_i(A,\Gamma,d_i,g)$ for $A=\Gamma=g=1$ and $d_1=\frac{3}{8}$, $d_2=\frac{1}{2}(3-\sqrt{5})$ are plotted in Figs. 3(a) and 3(b), respectively, along with the associated Voronoi polygons. The Voronoi polygon associated with a point P_i in a collection P of points in the plane consists of all points in the plane that are closer to P_i than any other point in P. The two values of d differ by less than 0.006 97, but the two pictures are dramatically different. One difference is in the shapes of the Voronoi polygons, all of which are of approximately equal area. For $d=\frac{3}{8}$, the polygons are more and more azimutally stretched farther from the origin, whereas for $d=\frac{1}{2}(3-\sqrt{5})$, they remain rough approximations of circles. Another difference becomes apparent when examining the neighbors of a given polygon. The points in Fig. 3 are numbered according to their distance from the origin. In Fig. 3(a), the number in any polygon differs from the numbers in the neighboring polygons by 3, 5, or 8. In Fig. 2(b), the differences are three consecutive members of the Fibonacci sequence $1,1,2,3,5,8,13,\ldots$, with transitions to higher numbers as one moves farther from the origin. It will become apparent that the contrast between these two examples is not merely due to the fact that one value of d is rational and the other is irrational. In the following, we will calculate the values of d that allow Voronoi tessellations such as that in Fig. 3(b). Our clue to understanding invariance is the appearance of the increasing members of the Fibonacci sequence for the case $d=\frac{1}{2}(3-\sqrt{5})$.

D. Fibonacci-like sequences of lattice vectors

Given $\vec{x}_0,\vec{x}_1\in\mathbb{R}^n$, define a Fibonacci-like sequence by $\vec{x}_{\nu+1}=\vec{x}_\nu+\vec{x}_{\nu-1}$. A key to uncovering many properties of this sequence is the Fibonacci Q matrix which expresses the recursion relation in matrix form,

$$\text{for } Q=\begin{pmatrix}1&1\\1&0\end{pmatrix},\quad \begin{pmatrix}\vec{x}_{\nu+1}\\ \vec{x}_\nu\end{pmatrix}=Q^\nu\begin{pmatrix}\vec{x}_1\\ \vec{x}_0\end{pmatrix}. \tag{3}$$

Diagonalization of the Q matrix yields the relation $Q^\nu=MD^\nu M^{-1}$, where

$$M=\begin{pmatrix}\phi_+&\phi_-\\1&1\end{pmatrix},\quad D=\begin{pmatrix}\phi_+&0\\0&\phi_-\end{pmatrix},$$

and $\phi_\pm=\frac{1\pm\sqrt{5}}{2}$ are the roots of $\eta^2-\eta-1=0$. Then, Eq. (3) is rewritten as

$$\begin{pmatrix}\vec{x}_{\nu+1}\\ \vec{x}_\nu\end{pmatrix}=Q^\nu\begin{pmatrix}\vec{x}_1\\ \vec{x}_0\end{pmatrix}=\frac{1}{\sqrt{5}}\begin{pmatrix}\phi_+^{\nu+1}-\phi_-^{\nu+1}&\phi_+^\nu-\phi_-^\nu\\ \phi_+^\nu-\phi_-^\nu&\phi_+^{\nu-1}-\phi_-^{\nu-1}\end{pmatrix}\begin{pmatrix}\vec{x}_1\\ \vec{x}_0\end{pmatrix}.$$

This gives *Binet's formula*,

$$\vec{x}_\nu=\frac{1}{\sqrt{5}}[(\phi_+^\nu-\phi_-^\nu)\vec{x}_1+(\phi_+^{\nu-1}-\phi_-^{\nu-1})\vec{x}_0]. \tag{4}$$

Motivated by our observations of cylindrical lattices in the annulus, we define a sequence Ω_ν of lattice basis matrices.

Ω_1 is defined by the four lattice constants A,Γ,d,g and integers m_0,m_1,q_0,q_1 such that $q_1m_0-q_0m_1=\gcd(m_0,m_1)=g$. $\Omega_1(A,\Gamma,d)$ will be understood within the context of given integers g,m_0,m_1,q_0,q_1 (so that we write it only as a function of A,Γ,d) and is defined by

$$\Omega_1(A,\Gamma,d) \doteq \sqrt{A}\begin{pmatrix} \frac{m_1}{\Gamma} & \frac{\Gamma}{g}(m_1d-q_1) \\ \frac{m_0}{\Gamma} & \frac{\Gamma}{g}(m_0d-q_0) \end{pmatrix}.$$

The sequence Ω_ν is then defined by

$$\Omega_\nu \doteq Q\Omega_{\nu-1} \quad \text{for} \quad \nu>1.$$

Choosing $\vec{x}_0=(q_0,m_0)$, $\vec{x}_1=(q_1,m_1)$ in Eq. (3), sequences $\{q_\nu\}$, $\{m_\nu\}$ are given by

$$\begin{pmatrix} q_{\nu+1} & m_{\nu+1} \\ q_\nu & m_\nu \end{pmatrix} = Q^\nu \begin{pmatrix} q_1 & m_1 \\ q_0 & m_0 \end{pmatrix}.$$

Noting that $\det Q^\nu=(-1)^\nu$ and taking the determinant of both sides of this last expression yield the relation

$$q_{\nu+1}m_\nu - q_\nu m_{\nu+1} = (-1)^\nu(q_1m_0-q_0m_1) = (-1)^\nu g.$$

Thus,

$$\Omega_\nu(A,\Gamma,d) = \sqrt{A}\begin{pmatrix} \frac{m_\nu}{\Gamma} & \frac{\Gamma}{g}(m_\nu d-q_\nu) \\ \frac{m_{\nu-1}}{\Gamma} & \frac{\Gamma}{g}(m_{\nu-1}d-q_{\nu-1}) \end{pmatrix},$$

where $g=q_1m_0-q_0m_1=(-1)^\nu(q_{\nu+1}m_\nu-q_\nu m_{\nu+1})$.

The eigenvectors of Q are $(\phi_+,1)^T$ (with eigenvalue ϕ_+) and $(\phi_-,1)^T$ (with eigenvalue ϕ_-). Since $\phi_+>1$ and $|\phi_-|<1$ for $x_0,x_1\in\mathbb{R}$, $|x_n|\to\infty$ unless the vector $(x_1,x_0)^T$ lies in the ϕ_- eigenspace or, equivalently, unless $x_1/x_0=\phi_-$. The second column of Ω_ν is in the ϕ_- eigenspace of Q if $(m_\nu d-q_\nu)/(m_{\nu-1}d-q_{\nu-1})=\phi_-$, that is, if

$$d = \frac{q_{\nu-1}+q_\nu\phi_+}{m_{\nu-1}+m_\nu\phi_+}.$$

Like $g=(-1)^\nu(q_{\nu+1}m_\nu-q_\nu m_{\nu+1})$, this last expression turns out to be independent of ν.

Proposition 1. Given two Fibonacci-like sequences of real numbers q_ν and m_ν generated by q_0,q_1 and m_0,m_1, respectively,

$$\frac{q_\nu+q_{\nu+1}\phi_+}{m_\nu+m_{\nu+1}\phi_+} = \frac{q_0+q_1\phi_+}{m_0+m_1\phi_+}$$

for all $\nu\in\mathbb{N}$.

Proof: The Q matrix has left eigenvector $(\phi_+,1)$ with eigenvalue ϕ_+. On the one hand then,

$$(\phi_+,1)\begin{pmatrix}1&1\\1&0\end{pmatrix}^\nu\begin{pmatrix}q_1&m_1\\q_0&m_0\end{pmatrix} = \phi_+^\nu(\phi_+,1)\begin{pmatrix}q_1&m_1\\q_0&m_0\end{pmatrix} = \phi_+^\nu(q_0+q_1\phi_+,m_0+m_1\phi_+).$$

On the other hand,

$$(\phi_+,1)\begin{pmatrix}1&1\\1&0\end{pmatrix}^\nu\begin{pmatrix}q_1&m_1\\q_0&m_0\end{pmatrix} = (\phi_+,1)\begin{pmatrix}q_{\nu+1}&m_{\nu+1}\\q_\nu&m_\nu\end{pmatrix} = (q_\nu+q_{\nu+1}\phi_+,m_\nu+m_{\nu+1}\phi_+).$$

Equating the two computations and dividing one by the other, we find that

$$\frac{\phi_+^\nu}{\phi_+^\nu}\frac{q_0+q_1\phi_+}{m_0+m_1\phi_+} = \frac{q_\nu+q_{\nu+1}\phi_+}{m_\nu+m_{\nu+1}\phi_+}.$$

Defining $\hat{d}(m_0,m_1,q_0,q_1)=(q_0+q_1\phi_+)/(m_0+m_1\phi_+)$, we have shown that for all $\nu\in\mathbb{N}$,

$$\frac{m_{\nu+1}\hat{d}-q_{\nu+1}}{m_\nu\hat{d}-q_\nu} = \phi_-,$$

and the second column of the matrix

$$\hat{\Omega}_\nu(A,\Gamma) = \Omega_\nu(A,\Gamma,d=\hat{d})$$

lies in the ϕ_- eigenspace of Q.

E. Discrete lattice invariance

Growth of the mean radius of the annular generative region or change in the van Iterson parameter from Γ to Γ' may be encoded in the growth matrix

$$G(\Gamma') = \begin{pmatrix} \frac{1}{\Gamma'} & 0 \\ 0 & \Gamma' \end{pmatrix},$$

so that $\Omega_\nu(A,\Gamma,d,g)G(\Gamma')=\Omega_\nu(A,\Gamma\Gamma',d,g)$. The results in Sec. II D may now be expressed as the following:

Observation. Discrete invariance under the scaling $\Gamma\to\Gamma\phi_+$,

$$Q\hat{\Omega}_\nu(A,\Gamma)G(\phi_+) \simeq \hat{\Omega}_\nu(A,\Gamma)\times\begin{pmatrix}1&0\\0&-1\end{pmatrix} \text{ and } Q^2\hat{\Omega}_\nu(A,\Gamma)G(\phi_+^2) \simeq \hat{\Omega}_\nu(A,\Gamma)$$

or, for any integer n,

$$Q\hat{\Omega}_\nu(A,\Gamma)G(\phi_+^n) \simeq \hat{\Omega}_\nu(A,\Gamma)\begin{pmatrix}1&0\\0&-1\end{pmatrix}^n.$$

That is, growth in Γ by a multiplicative factor ϕ_+, accompanied by a change of basis through Q, preserves the lattice basis up to a change in orientation.

The calculation of the relations is as follows:

$$Q\hat{\Omega}_\nu G(\phi_+) = Q\sqrt{A}\begin{pmatrix} \frac{m_\nu}{\Gamma} & \frac{\Gamma}{g}(m_\nu d - q_\nu) \\ \frac{m_{\nu-1}}{\Gamma} & \frac{\Gamma}{g}(m_{\nu-1}d - q_{\nu-1}) \end{pmatrix} G(\phi_+)$$

$$= \sqrt{A}\begin{pmatrix} \frac{m_{\nu+1}}{\Gamma} & \phi_- \frac{\Gamma}{g}(m_\nu d - q_\nu) \\ \frac{m_\nu}{\Gamma} & \phi_- \frac{\Gamma}{g}(m_{\nu-1}d - q_{\nu-1}) \end{pmatrix} G(\phi_+)$$

$$= \sqrt{A}\begin{pmatrix} \frac{1}{\phi_+}\frac{m_{\nu+1}}{\Gamma} & \phi_+\phi_- \frac{\Gamma}{g}(m_\nu d - q_\nu) \\ \frac{1}{\phi_+}\frac{m_\nu}{\Gamma} & \phi_+\phi_- \frac{\Gamma}{g}(m_{\nu-1}d - q_{\nu-1}) \end{pmatrix}$$

$$\simeq \Omega_\nu(A,\Gamma)\begin{pmatrix} 1 & 0 \\ 0 & -1 \end{pmatrix}.$$

The last simequality comes from noting that $\phi_+\phi_- = -1$ and $m_{\nu+1}/\phi_+ \simeq m_\nu$. The latter relation is a consequence of the limit, $\lim_{\nu\to\infty}(m_{\nu+1}/m_\nu) = \phi_+$, which is proven by inspection of Binet's formula while remembering that $|\phi_-|^\nu$ is small for large ν. The convergence is typically (and in particular for the Fibonacci sequence $m_\nu = f_\nu$) quick, so that we can write $m_{\nu+1}/m_\nu \simeq \phi_+$. This invariance is illustrated in Fig. 2, where the lattice points correspond to the maxima of the graphed function.

F. Rational approximations of noble numbers

In the classical theory of continued fraction expansions of real numbers, the numbers $(q_0+q_1\phi_+)/(m_0+m_1\phi_+)$, where the integers q_0, q_1, m_0, m_1 satisfy $q_1m_0 - q_0m_1 = \pm 1$, carry the distinguished title *noble numbers*. Hotton *et al.* [15] studied their relation to hyperbolic geometry and the van Iterson diagram (which relates the van Iterson parameter to the divergence angle), and the noble numbers and their special continued fraction expansions appear in numerous studies of phyllotaxis [18,28,32,34–36]. In this section, we relate the invariance results of Sec. II E to the classical theory of continued fraction expansions and derive thereby a formula for the hyperbolic curves in Fig. 2.

We begin with a brief overview of continued fraction expansions with reference to theorems proved by Hardy and Wright [13]. Any $\xi \in \mathbb{R}$ has a unique continued fraction expansion

$$\xi = a_0 + \cfrac{1}{a_1 + \cfrac{1}{a_2 + \cfrac{1}{a_3 + \cdots + \cfrac{1}{a_n + \cdots}}}},$$

where $a_0 \in \mathbb{Z}$ and $a_i \in \mathbb{N}$ for $i \geq 1$. The right-hand side is more compactly written as $\xi = [a_0, a_1, a_2, \ldots]$, and the equality means that the sequence

$$\frac{p_\nu}{z_\nu} = [a_0, a_1, \ldots, a_\nu, 0, 0, \ldots] \doteq [a_0, a_1, \ldots, a_\nu]$$

of rational numbers converges to ξ. Now suppose that $\xi \in \mathbb{R} - \mathbb{Q}$. The number p_ν/z_ν, called the νth *convergent* to ξ, is the best rational approximation of ξ in that if $n > 1$, $0 < z < z_\nu$, and $p/z \neq p_\nu/z_\nu$, then

$$\left|\frac{p_\nu}{z_\nu} - \xi\right| < \left|\frac{p}{z} - \xi\right|$$

([13], Theorem 181). Furthermore, the quality of the approximation p_ν/z_ν is estimated in terms of z_ν and $a_{\nu+1}$ by the inequality

$$\left|\frac{p_\nu}{z_\nu} - \xi\right| < \frac{1}{z_\nu^2 a_{\nu+1}} \tag{5}$$

([13], p. 163). An irrational number ξ can thus be approximated by rationals' best if the integers a_ν are large.

Two numbers $\xi, \eta \in \mathbb{R}$ are said to be *equivalent* if the continued fraction expansion for ξ after some term a_μ is the same as the expansion of η after some term b_ν, i.e.,

$$\xi = [a_0, a_1, \ldots, a_\mu, c_0, c_1, \ldots],$$

$$\eta = [b_0, b_1, b_2, \ldots, b_\nu, c_0, c_1, \ldots].$$

This condition is an equivalence relation on $\mathbb{R}$ and can be expressed as

$$\xi = \frac{q_0 + q_1\eta}{m_0 + m_1\eta}$$

for integers q_i, m_i such that $q_1m_0 - q_0m_1 = \pm 1$ ([13], Theorem 73). The number ϕ_+ has the continued fraction expansion $\phi_+ = [1, 1, 1, \ldots]$ and the numbers $(q_0+q_1\phi_+)/(m_0+m_1\phi_+)$ (with $q_0m_1 - m_0q_1 = \pm 1$) in its equivalence class are in the sense of Eq. (5), the most difficult irrational numbers to approximate by rationals. However, an infinite number of rational approximations will satisfy an inequality which, for ϕ_+ and the members of its equivalence class, is stronger than Eq. (5). Any irrational ξ also has an infinite number of rational approximations $\frac{p}{z}$ which satisfy ([13], Theorem 185)

$$\left|\frac{p}{z} - \xi\right| < \frac{1}{z^2\sqrt{5}}.$$

Rewritten,

$$z|z\xi - p| < \frac{1}{\sqrt{5}}. \tag{6}$$

This is the best possible result in that $\sqrt{5}$ cannot be replaced by any larger number. Specifically, Hardy and Wright showed that for $\xi = \phi_+$, the assumption that an infinite number of rationals $\frac{p}{z}$ satisfy an inequality $|\frac{p}{z} - \xi| < 1/z^2\eta$ (that is, $z|z\xi - p| < \frac{1}{\eta}$) for $\eta > \sqrt{5}$ leads to a contradiction. From this we can conclude that there is a sequence of rationals p_ν/z_ν such that $z_\nu|z_\nu\phi_+ - p_\nu|$ converges to $\frac{1}{\sqrt{5}}$ from below. A similar conclusion can be reached for any of the noble numbers.

The numbers q_ν/m_ν are not, in general, the νth convergents to $\hat{d}(m_0, m_1, q_0, q_1) = (q_0+q_1\phi_+)/(m_0+m_1\phi_+)$, but using

Binet's formula one can show that they do converge to $\hat{d}$,

$$\lim_{\nu\to\infty}\frac{q_\nu}{m_\nu}=\frac{q_0+q_1\phi_+}{m_0+m_1\phi_+}.$$

Inspired by Eq. (6), we calculate the quantities $m_\nu(m_\nu\hat{d}-q_\nu)$ and arrive at the following:

Proposition 2. Given two Fibonacci-like sequences q_ν and m_ν generated by q_0,q_1 and m_0,m_1, respectively, define $g\doteq q_1m_0-q_0m_1$ and $\hat{d}\doteq(q_0+q_1\phi_+)/(m_0+m_1\phi_+)$. Then,

$$\lim_{k\to\infty}\frac{m_{2k}}{g}(m_{2k}\hat{d}-q_{2k})=\frac{1}{\sqrt{5}}$$

and

$$\lim_{k\to\infty}\frac{m_{2k+1}}{g}(m_{2k+1}\hat{d}-q_{2k+1})=-\frac{1}{\sqrt{5}}.$$

Proof 1: Using Binet's formula to express m_ν,q_ν in terms of m_0,m_1,q_0,q_1, write

$$\frac{m_\nu}{q_1m_0-q_0m_1}\left(m_\nu\frac{q_0+q_1\phi_+}{m_0+m_1\phi_+}-q_\nu\right)=\frac{(-1)^\nu(m_0+m_1\phi_+)+\phi_-^{2\nu-2}(m_0+m_1\phi_-)}{\sqrt{5}(m_0+m_1\phi_+)}.$$

Now note that $|\phi_-|<1$.

A second proof makes use of the ν-invariant nature of g and $\hat{d}$.

Proof 2:

$$\begin{aligned}\frac{m_\nu}{g}(m_\nu\hat{d}-q_\nu)&=\frac{m_\nu}{q_1m_0-q_0m_1}\left(m_\nu\frac{q_0+q_1\phi_+}{m_0+m_1\phi_+}-q_\nu\right)\\&=(-1)^\nu\frac{m_\nu}{q_{\nu+1}m_\nu-q_\nu m_{\nu+1}}\left(m_\nu\frac{q_\nu+q_{\nu+1}\phi_+}{m_\nu+m_{\nu+1}\phi_+}-q_\nu\right)\\&=(-1)^\nu\frac{m_\nu}{q_{\nu+1}m_\nu-q_\nu m_{\nu+1}}\left(\frac{(q_{\nu+1}m_\nu-q_\nu m_{\nu+1})\phi_+}{m_\nu+m_{\nu+1}\phi_+}\right)\\&=\frac{m_\nu\phi_+}{m_\nu+m_{\nu+1}\phi_+}\\&=(-1)^\nu\frac{\phi_+}{1+\frac{m_{\nu+1}}{m_\nu}\phi_+}.\end{aligned}$$

The limit $\lim_{\nu\to\infty}(m_{\nu+1}/m_\nu)=\phi_+$ and equalities $|\phi_-|=\frac{1}{\phi_+}=1+\phi_+^2$ and $|\phi_-|+\phi_+=\sqrt{5}$ complete the proof.

Note also that for $d\neq\hat{d}(m_0,m_1,q_0,q_1)$, the sequence $|(m_\nu/g)(m_\nu d-q_\nu)|$ diverges. Proposition 2 holds for any $q_0,q_1,m_0,m_1\in\mathbb{R}$, but in the context of cylindrical lattices, we take $m_0,m_1\in\mathbb{N}$ and choose $q_0,q_1\in\mathbb{Z}$ such that $q_1m_0-q_0m_1=\gcd(m_0,m_1)=g$.

For the classical Fibonacci sequence, it is convenient to take $m_0=0$, $m_1=1$. Then, $\gcd(m_0,m_1)$ is not defined, but for $q_0=-1$, $q_1=1$, $q_0m_1-q_1m_0=1$, and $q_\nu m_{\nu+1}-q_{\nu+1}m_\nu=(-1)^\nu=(-1)^\nu\gcd(m_\nu,m_{\nu+1})$ for $\nu\geq1$. Writing f_ν for the νth (classical) Fibonacci number, $m_\nu=f_\nu$ and $q_\nu=f_{\nu-1}$. Proposition 2 tells us to consider the special value $d=(-1+\phi_+)/(0+\phi_+)=1+\phi_-$ and gives us the limit

$$\lim_{\nu\to\infty}f_\nu|f_\nu(1+\phi_-)-f_{\nu-2}|=\frac{1}{\sqrt{5}}.$$

Consider now the matrix $\hat{\Omega}_\nu$ in light of Proposition 2. Defining $\rho_\nu\doteq\Gamma/m_\nu$,

$$\hat{\Omega}_\nu(A,\Gamma)=\sqrt{A}\begin{pmatrix}\frac{1}{\rho_\nu} & \rho_\nu\frac{1}{g}m_\nu(m_\nu\hat{d}-q_\nu)\\ \frac{1}{\rho_{\nu-1}} & \rho_{\nu-1}\frac{1}{g}m_{\nu-1}(m_{\nu-1}\hat{d}-q_{\nu-1})\end{pmatrix}\simeq\sqrt{A}\begin{pmatrix}\frac{1}{\rho_\nu} & \rho_\nu\frac{\pm1}{\sqrt{5}}\\ \frac{1}{\rho_{\nu-1}} & \rho_{\nu-1}\frac{\mp1}{\sqrt{5}}\end{pmatrix}.$$

This tells us that the sequence $\vec{\omega}_\nu$ of basis vectors lies near the curves $\sqrt{A}(\frac{1}{\rho},\pm\frac{\rho}{\sqrt{5}})$ parametrized by ρ. These curves, illustrated in Fig. 2, give a continuous invariance in that lattice vectors lie near these curves for all values of R.

III. PLANFORM INVARIANCE

In Sec. II F, we described phyllotactic lattices. Actual plant surfaces are, however, three-dimensional structures—deformations of a disk or sphere into surfaces with peaks and valleys. The peaks correspond to the centers of the primordia and give the lattice points; the valleys trace out the tiles. In this section, we describe plant surfaces in terms of functions $w(s,\theta)$ that are periodic with respect to a cylindrical lattice $\mathbb{L}$. Amplitudes and wave vectors of a Fourier representation of function $w(s,\theta)$ may be calculated from PDE models, as described in Sec. III B. Properties of solutions of amplitude equations derived from the PDEs are derived in Secs. III C and III D for discretely varying values of R and in Sec. III E for continuously varying R.

A. Lattice-periodic functions and dual lattice

Given a lattice $\mathbb{L}=\{z_1\vec{v}+z_2\vec{w}:(z_1,z_2)\in\mathbb{Z}^2\}$, a function $w(\vec{x})$ is $\mathbb{L}$ periodic if $w(\vec{x}+\vec{\omega})=w(\vec{x})$ for all $\vec{x}\in\mathbb{R}^2$ and $\vec{\omega}\in\mathbb{L}$ or, equivalently, if for all $\vec{x}\in\mathbb{R}^2$

$$w(\vec{x}+\vec{v})=w(\vec{x}+\vec{w})=w(\vec{x}).$$

Denoting the space of smooth real-valued $\mathbb{L}$-periodic functions by $C^\infty_{\mathbb{L}}(\mathbb{R}^2,\mathbb{R})$, any $w\in C^\infty_{\mathbb{L}}(\mathbb{R}^2,\mathbb{R})$ has a Fourier series expansion

$$w(\vec{x})=\sum_{(z_1,z_2)\in\mathbb{Z}^2}A_{(z_1,z_2)}e^{i(z_1\vec{k}_m+z_2\vec{k}_n)\cdot\vec{x}},\quad A_{(-z_1,-z_2)}=A^*_{(z_1,z_2)}\tag{7}$$

for complex amplitudes $A_{(z_1,z_2)}$. The condition $A_{(-z_1,-z_2)}=A^*_{(z_1,z_2)}$, where * denotes the complex conjugate,

insures that w is real valued. The vectors $\vec{k}_m$, $\vec{k}_n$ are a basis for the dual lattice $\mathbb{K}$ to $\mathbb{L}$.

The determination of wave vectors and amplitudes from PDE models for phyllotaxis will be described in Sec. III C. The radius R will be a parameter in those equations, and we will solve for the lattice coordinates d and A. As $\Gamma=\frac{2\pi R}{A}$ depends on both R and A, it will be convenient to work with the lattice $\mathbb{L}(A,R,d,g)$ with basis matrix $\Omega_{m,n}(A,R,d,g)$ given by Eq. (1), that is,

$$\Omega_{(m,n)}(A,R,d,g)=\begin{pmatrix}\frac{A}{2\pi}\frac{n}{R} & \frac{2\pi R}{g}(nd-p)\\ \frac{A}{2\pi}\frac{m}{R} & \frac{2\pi R}{g}(md-q)\end{pmatrix}=\begin{pmatrix}\frac{A}{2\pi}\frac{1}{\rho_n} & -2\pi\rho_n\delta_n\\ \frac{A}{2\pi}\frac{1}{\rho_m} & -2\pi\rho_m\delta_m\end{pmatrix},$$

where $\rho_m=\frac{R}{m}$, $\delta_m=\frac{m}{g}(q-md)$, $\rho_n=\frac{R}{n}$, and $\delta_n=\frac{n}{g}(p-nd)$. The dual vectors $\vec{k}_m$, $\vec{k}_n$ are given by

$$(-\vec{k}_m^t\vec{k}_n^t)=K=2\pi\Omega^{-1}=\begin{pmatrix}-\frac{(2\pi)^2}{A}\rho_m\delta_m & \frac{(2\pi)^2}{A}\rho_n\delta_n\\ -\frac{1}{\rho_m} & \frac{1}{\rho_n}\end{pmatrix}.$$

The dual vectors are thus

$$\vec{k}_m=\left(\frac{(2\pi)^2}{A}\rho_m\delta_m,\frac{1}{\rho_m}\right),\quad \vec{k}_n=\left(\frac{(2\pi)^2}{A}\rho_n\delta_n,\frac{1}{\rho_n}\right).\tag{8}$$

In analogy to the Fibonacci-like sequence $\vec{\omega}_\nu$, we define a Fibonacci-like sequence

$$\vec{k}_\nu=\left(\frac{(2\pi)^2}{A}\rho_\nu\delta_\nu,\frac{1}{\rho_\nu}\right),\tag{9}$$

where $\rho_\nu=m_\nu/R$ and $\delta_\nu=(m_\nu/g)(q_\nu-m_\nu d)$. Proposition 2 tells us that in the limit of increasing ν, the dual basis vectors $\vec{k}_\nu$ evaluated at $d=\hat{d}$ lie close to the curves $(\pm\rho[(2\pi)^2/\sqrt{5}A],1/\rho)$.

B. PDE models for phyllotactic patterning

Many phenomena in nature and in the laboratory give rise to planforms of diamonds, hexagons, or ridges [6]. Examples include Rayleigh-Bènard convection experiments, the Rosenzweig instability in ferrofluids [11], and geological formations [22]. In all of these systems, an initially homogeneous state is broken to a state of discrete symmetry as a control parameter crosses a threshold value. The resulting pattern is determined by universal symmetries as well as details of the mechanism. The latter influence, for example, the winning configuration in the competition between hexagons and ridges and determine the length scale of the pattern. In [25], we show how models that have been proposed for biophysical mechanism for primordium formation (in which, following the hypothesis of Green [12], primordia arise due to buckling induced by compressive stresses that result from differential growth) and biochemical mechanisms (in particular, the diffusion and transport by PIN1 proteins of the growth hormone auxin, as proposed by Kuhlemeier and coworkers; see Kuhlemeier and co-workers [30,31,40] and Jönsson *et al.* [20] for experiments and models) have similar mathematical form and can be analyzed by reduction to similar sets of differential equations for the wave vectors $\vec{k}_\nu$ and amplitudes A_ν of periodic functions. If w represents the normal deflection of the buckling plant tunica (in the biophysical model) or auxin concentration (in a biochemical model), we explain how the equation

$$w_t+\Delta^2 w+P\Delta w+\Lambda^4 w+\text{nonlinear terms}=0\tag{10}$$

for constants P and Λ^4 captures both models. The linear terms differ only in the interpretation of the parameters, and quadratic nonlinearities are present in both models. The parameter P is the control parameter, representing compressive stress in the biophysical model and the relative strength of auxin transport to diffusion in the biochemical model. For large enough P, the homogeneous solution $w=0$ becomes unstable to a solution that depends on both the nonlinear and linear terms in the equation. Depending on the nonlinear terms, Eq. (10) may or may not be gradient [that is, the solution may or may not minimize an energy functional $\mathfrak{E}(w)$]. The elastic energy plays the role of $\mathfrak{E}$ for a mechanical buckling model. Whereas there is no reason to assume that a biochemical mechanism would be gradient, an energy $\mathfrak{E}(w)$ may still be relevant near the threshold of pattern formation.

In our analysis of the model PDEs, we make in [25,38,39] the ansatz that w is an $\mathbb{L}$-periodic function for some lattice $\mathbb{L}$ with dual lattice $\mathbb{K}$, so that w has form (7). The dual lattice vectors $\vec{k}_m$ and $\vec{k}_n$ can be functions of the spatial coordinates, so that $\mathbb{L}$ should be viewed as a local lattice. Spatial dependence of the wave vectors is necessary if, for example, the radius R changes or if defects occur in the pattern. We begin here, however, with a simple case. We assume that our PDE model (10) has an energy $\mathfrak{E}(w)$ and make the ansatz that w has form (7), where the sum is restricted to wave vectors $\vec{k}=z_1\vec{k}_m+z_2\vec{k}_n$ in the active set $\mathfrak{A}$. The active set consists of those wave vectors $\vec{k}$ for which the linear growth rate $\sigma(\vec{k})$ is positive or slightly negative, say greater than a constant σ_c. Minimization of $\mathfrak{E}(w)$ over functions of form (7) reduces to the minimization of an energy functional $\mathfrak{E}(\vec{k}_m,\vec{k}_n;\{A_{\vec{k}}\})$ over the wave-vector basis $\vec{k}_m,\vec{k}_n$ and associated amplitudes $A_{\vec{k}}$, where $\vec{k}\in\mathfrak{A}\cap\mathbb{L}$; $\mathbb{L}=\{z_1\vec{k}_m+z_2\vec{k}_n:z_1,z_2\in\mathbb{N}\}$. We calculate from a biophysical model in [38,39] and from a biochemical model in [25] an energy of the form

$$\mathfrak{E}(\vec{k}_m,\vec{k}_n;\{A_{\vec{k}}\})=-\sum_{\vec{k}\in\mathfrak{A}\cap\mathbb{L}}\sigma(\vec{k})A_{\vec{k}}A_{\vec{k}}^*-\sum_{\vec{k}_a+\vec{k}_b+\vec{k}_c=0}\tau(\vec{k}_a,\vec{k}_b,\vec{k}_c)\times(A_aA_bA_c+A_a^*A_b^*A_c^*)+\gamma\left(\frac{1}{2}\sum_{\vec{k}\in\mathfrak{A}\cap\mathbb{L}}A_{\vec{k}}^2A_{\vec{k}}^{*2}+2\sum_{\vec{k}_p\neq\vec{k}_q}A_pA_p^*A_qA_q^*\right).\tag{11}$$

Note that the cubic term is summed over all $\vec{k}_a,\vec{k}_b,\vec{k}_c$ in $\mathfrak{A}\cap\mathbb{L}$ such that $\vec{k}_\nu+\vec{k}_p+\vec{k}_q=0$. We emphasize that Eq. (11) is universal in form in that any system with quadratic and cubic nonlinearities (in the PDE, that is, cubic or quartic nonlinearities in the energy functional) differs from Eq. (11) only in the coefficients σ,τ,γ. These coefficients depend on the parameters in the original PDE as well as the wave vectors and thus contain information specific to the particular mechanism under investigation.

For the linear terms given in Eq. (10),

$$\sigma(\vec{k}) = -k^4 + 2Pk^2 - \Lambda^4, \tag{12}$$

where $k^2=\|\vec{k}\|^2$. For $P=P_c=1$, $\sigma(\vec{k})=0$ for wave vectors of length Λ, whereas all other wave vectors have negative growth rates. For P slightly larger than P_c, there is an annulus of wave vectors with mean radius Λ for which $\sigma(\vec{k}_c)>0$. The set of active modes in this case of near-onset ($P\simeq P_c$) instability is thus an annulus in wave-vector space. (In a biomechanical model, the stress state may be nonisotropic, so that only a subset of this annulus is the active set. We consider only the isotropic case here.)

The wave vectors in the wave-vector lattice $\mathbb{L}$ are parametrized by the four lattice constants A,R,d,g and the natural numbers m,n. The radius R of the cylinder (or average radius of the generative region in case the pattern is forming on a noncylindrical geometry) is an external parameter, not chosen by energy minimization, and m,n determine g, so that $\mathfrak{E}(\vec{k}_m,\vec{k}_n;\{A_{\vec{k}}\})$ can be treated as an energy $\mathfrak{E}(A,d,m,n;\{A_{\vec{k}}\})$ or as an energy $\mathfrak{E}(l_m,l_n,m,n;\{A_{\vec{k}}\})$, where $l_m=[(2\pi)^2/A]\rho_m\delta_m$ and $l_n=[(2\pi)^2/A]\rho_n\delta_n$ are the radial wave numbers. Our task is to find the choices of A, d, m, n, and $A_{\vec{k}}$ that minimize this energy. This may be accomplished via the following algorithm:

(1) *Determination of the set* $\mathfrak{A}$. As described above, in our near-onset analysis, we take $P\simeq P_c$, choose a threshold σ_c, and obtain an active set $\mathfrak{A}$ that is an annulus in wave-vector space. The choice of R fixes the mean radius of the annular generative region. We assume that the radial width of the generative region is larger than the pattern wavelength so that the pattern is determined by minimization of the energy $\mathfrak{E}$ without radial boundary conditions.

(2) *Optimal planform for given* m,n. For any choice of integers m,n, the associated wave vectors are given by Eq. (8). For only a finite set of m,n do the angular wave numbers $1/\rho_m=R/m$ and $1/\rho_n=R/n$ lie in $\mathfrak{A}$ for some choice of radial wave numbers l_m,l_n. Solving the equations

$$\frac{\partial\mathfrak{E}}{\partial d}=0,\quad \frac{\partial\mathfrak{E}}{\partial A}=0,\quad \frac{\partial\mathfrak{E}}{\partial A_{\vec{k}}}=0 \text{ or } \frac{\partial\mathfrak{E}}{\partial l_m}=0,\quad \frac{\partial\mathfrak{E}}{\partial l_n}=0,\quad \frac{\partial\mathfrak{E}}{\partial A_{\vec{k}}}=0 \tag{13}$$

for d,A or l_m,l_n and the amplitudes $A_{\vec{k}}$ gives us optimal planform (7) for this choice of m,n.

(3) *Optimal choice of* m,n. The energies $\mathfrak{E}(d,A,m,n;\{A_{\vec{k}}\})$ associated with the optimal configurations computed in step 3 for varying (m,n) are compared. The lowest energy corresponds to the optimal choice of m,n and the ideal configuration.

C. Discrete shape invariance

If the radius R influences only the geometry of the problem and no features of the mechanism (such as diffusion or transport rates of chemicals or stiffness of the plant tunica), then the energy $\mathfrak{E}$ depends on R exclusively through the quantities $\rho_m=\frac{R}{m}$ and $\rho_n=\frac{R}{n}$. We may then write an energy $\mathfrak{E}(l_m,l_n,\rho_m,\rho_n;\{A_{\vec{k}}\})$ that only depends on R through ρ_m,ρ_n. How do we interpret an energy-minimizing solution with wave vectors $\vec{k}_m=(l_m,1/\rho_m)$ and $\vec{k}_n=(l_n,1/\rho_n)$? For a given choice of R,m_0,m_1 such that $\rho_m=R/m_0$ and $\rho_n=R/m_1$, consider the Fibonacci-like sequence $\{m_\nu\}$ generated by m_0 and m_1. The sequence $\{m_{\nu+1}/m_\nu\}$ converges (quickly) to ϕ_+, so let us assume that $m_1/m_0\simeq\phi_+$. This implies that $\rho_m=R/m_0\simeq R\phi_+/m_1$ and $\rho_n=R/m_1\simeq R\phi_+/m_2$. More generally,

$$\rho_m\simeq\frac{R\phi_+^\nu}{m_\nu}\quad\text{and}\quad\rho_n\simeq\frac{R\phi_+^\nu}{m_{\nu+1}}.$$

One solution with wave vectors $\vec{k}_m$, $\vec{k}_n$ thus gives rise to a sequence of solutions with wave vectors

$$\vec{k}_m=\left(l_m,\frac{m_\nu}{R\phi_+^\nu}\right),\quad \vec{k}_{\nu+1}=\left(l_n,\frac{m_{\nu+1}}{R\phi_+^\nu}\right)$$

and amplitudes

$$A_m(R)=A_{m_\nu}(R\phi_+^\nu),\quad A_n(R)=A_{m_{\nu+1}}(R\phi_+^\nu).$$

In other words, the solution to the problem for a given value of R is nearly identical to the solution for the values $R\phi_+^\nu$ for the appropriate values of m_ν. This is illustrated in Fig. 2, where planforms corresponding to hexagonal- and square-lattice solutions as discussed in Sec. III D are plotted for values of R in multiples of ϕ_+.

The amplitudes are also functions of R/m_ν, so that

$$A_{m_\nu}(R)=A\left(\frac{R}{m_\nu}\right)=A\left(\frac{R\phi_+}{m_\nu\phi_+}\right)=A_{m_{\nu+1}}(R\phi_+).$$

In Sec. III E, we will make use of the fact that the amplitudes

$$A_{m_\nu}(R)=A\left(\frac{R}{m_\nu}\right)=A\left(\frac{R}{m_0\phi_+^\nu}\right) \tag{14}$$

may be considered to be functions of ν for given R and m_0.

D. Symmetries in the amplitude equations

Using expression (12) for $\sigma(k^2)$, assuming that $\tau(\vec{k}_a,\vec{k}_b,\vec{k}_c)=\tau(k_a^2,k_b^2,k_c^2)$ is a function of the moduli of the wave vectors, and taking the quartic coefficient γ in energy (11) to be constant (as it is in [25,38,39]), Eqs. (13) read

$$-\frac{\partial\mathfrak{E}}{\partial d}=\sum_{\vec{k}\in\mathfrak{A}\cap\mathbb{L}}2(P-k^2)\frac{\partial k^2}{\partial d}A_{\vec{k}}A_{\vec{k}}^*+\sum_{\vec{k}+\vec{k}_b+\vec{k}_c=0}\frac{\partial\tau(\vec{k},\vec{k}_b,\vec{k}_c)}{\partial k^2}\frac{\partial k^2}{\partial d}(A_{\vec{k}}A_bA_c+A_{\vec{k}}^*A_b^*A_c^*)=0, \tag{15a}$$

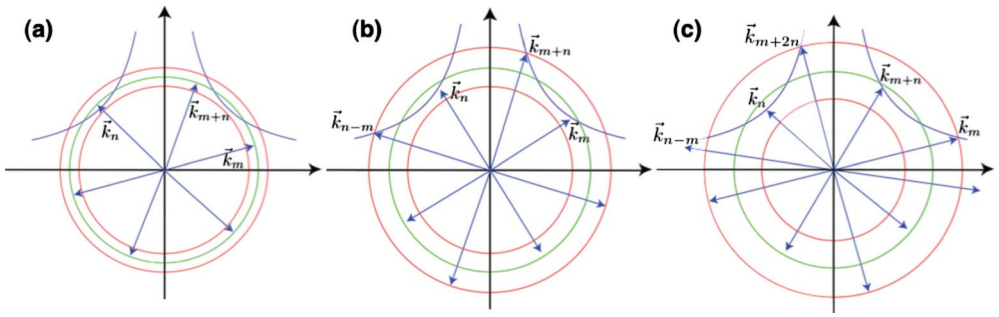

FIG. 4. (Color online) Illustrations of the active set $\mathfrak{A}$ of wave vectors. The circles of smallest and largest radii (in red) bound the active set. The wave vectors of maximum linear growth rate $\sigma(\vec{k})$ lie on the (green) circle of intermediate radius. More wave vectors of a lattice fit into the active set as the width increases. Illustrated are configurations with (a) one, (b) two overlapping, and (c) three overlapping triads of wave vectors. The curves $(\pm\rho[(2\pi)^2/\sqrt{5}A], \frac{1}{\rho})$ are also plotted.

$$-\frac{\partial \mathfrak{E}}{\partial A} = \sum_{\vec{k}\in\mathfrak{A}\cap\mathbb{L}} 2(P-k^2)\frac{\partial k^2}{\partial A}A_{\vec{k}}A^*_{\vec{k}} + \sum_{\vec{k}+\vec{k}_b+\vec{k}_c=0} \frac{\partial \tau(\vec{k},\vec{k}_b,\vec{k}_c)}{\partial k^2}\frac{\partial k^2}{\partial A}(A_{\vec{k}}A_bA_c + A^*_{\vec{k}}A^*_bA^*_c) = 0, \tag{15b}$$

$$-\frac{\partial \mathfrak{E}}{\partial A_{\vec{k}}} = \sigma(k^2)A_k + \sum_{\vec{k}+\vec{k}_b+\vec{k}_c=0} \tau(\vec{k},\vec{k}_b,\vec{k}_c)A_bA_c - \gamma(S - A_{\vec{k}}A^*_{\vec{k}}) = 0 \tag{15c}$$

or

$$-\frac{\partial \mathfrak{E}}{\partial l_m} = \sum_{\vec{k}\in\mathfrak{A}\cap\mathbb{L}} 2(P-k^2)\frac{\partial k^2}{\partial l_m}A_{\vec{k}}A^*_{\vec{k}} + \sum_{\vec{k}+\vec{k}_b+\vec{k}_c=0} \frac{\partial \tau(\vec{k},\vec{k}_b,\vec{k}_c)}{\partial k^2}\frac{\partial k^2}{\partial l_m}(A_{\vec{k}}A_bA_c + A^*_{\vec{k}}A^*_bA^*_c) = 0, \tag{16a}$$

$$-\frac{\partial \mathfrak{E}}{\partial l_n} = \sum_{\vec{k}\in\mathfrak{A}\cap\mathbb{L}} 2(P-k^2)\frac{\partial k^2}{\partial l_m}A_{\vec{k}}A^*_{\vec{k}} + \sum_{\vec{k}+\vec{k}_b+\vec{k}_c=0} \frac{\partial \tau(\vec{k},\vec{k}_b,\vec{k}_c)}{\partial k^2}\frac{\partial k^2}{\partial l_m}(A_{\vec{k}}A_bA_c + A^*_{\vec{k}}A^*_bA^*_c) = 0, \tag{16b}$$

$$-\frac{\partial \mathfrak{E}}{\partial A_{\vec{k}}} = \sigma(k^2)A_k + \sum_{\vec{k}+\vec{k}_b+\vec{k}_c=0} \tau(\vec{k},\vec{k}_b,\vec{k}_c)A_bA_c - \gamma(S - A_{\vec{k}}A^*_{\vec{k}}) = 0, \tag{16c}$$

where $S=2\Sigma_{\vec{k}\in\mathfrak{A}\cap\mathbb{L}}(A_{\vec{k}}A^*_{\vec{k}})$. The second summation in each equation is taken over all pairs of wave vectors $\vec{k}_b,\vec{k}_c$ in $\mathfrak{A}\cap\mathbb{L}$ such that $\vec{k}+\vec{k}_b+\vec{k}_c=0$. Since P is slightly larger than P_c and the active set $\mathfrak{A}$ is a narrow annulus, only a few triads $\vec{k}_a,\vec{k}_b,\vec{k}_c$ such that $\vec{k}_a+\vec{k}_b+\vec{k}_c=0$ are present in $\mathfrak{A}$. Figure 4 shows examples with increasing $P-P_c$ (and therefore increasing active annulus width) in which only one triad [Fig. 4(a); $\vec{k}_m+\vec{k}_n-\vec{k}_{m+n}=0$], two overlapping triads [Fig. 4(b); $\vec{k}_{n-m}+\vec{k}_m-\vec{k}_n=0$ and $\vec{k}_m+\vec{k}_n-\vec{k}_{m+n}=0$], or three overlapping triads [Fig. 4(c); $\vec{k}_{n-m}+\vec{k}_m-\vec{k}_n=0$, $\vec{k}_m+\vec{k}_n-\vec{k}_{m+n}=0$, and $\vec{k}_n+\vec{k}_{m+n}-\vec{k}_{m+2n}=0$] fit into the active annulus. We now discuss each of these cases. To simplify the expressions, we take τ to be independent of k^2; similar results apply if this is not the case.

1. Hexagons—The case of one triad

For one triad of wave vectors $\vec{k}_m,\vec{k}_n,\vec{k}_m+\vec{k}_n=\vec{k}_{m+n}$, as in Fig. 4(a), Eqs. (16), set equal to zero, are

$$l_m(P-k_m^2)A_mA^*_m + (l_m+l_n)(P-k^2_{m+n})A_{m+n}A^*_{m+n} = 0, \tag{17a}$$

$$l_n(P-k_n^2)A_nA^*_n + (l_m+l_n)(P-k^2_{m+n})A_{m+n}A^*_{m+n} = 0, \tag{17b}$$

$$\sigma_mA_m + \tau A^*_nA^*_{m+n} - \gamma A_m(S - A_mA^*_m) = 0, \tag{17c}$$

$$\sigma_nA_n + \tau A^*_mA^*_{m+n} - \gamma A_m(S - A_mA^*_m) = 0, \tag{17d}$$

$$\sigma_{m+n}A_{m+n} + \tau A^*_mA^*_n - \gamma A_{m+n}(S - A_{m+n}A^*_{m+n}) = 0, \tag{17e}$$

where $S=2(A_mA^*_m+A_nA^*_n+A_{m+n}A^*_{m+n})$ and, for example, $\sigma_m=\sigma(k^2_m)$. Equations (17a) and (17b) are solved if $k^2_m=k^2_n=k^2_{m+n}=P$. Then, $\sigma_m=\sigma_n=\sigma_{m+n}$ and the remaining three equations have the real-valued solution $A_m=A_n=A_{m+n}=(\tau\pm\sqrt{\tau^2+20\sigma\gamma})/10\gamma$. It is well known that, for $-1/20<\sigma\gamma/\tau^2<4/3$, this is a minimum of the energy functional (that is, a stable solution of the ODEs $dA_m/dt=-\partial\mathfrak{E}/\partial A_m$) [16]. Example solutions are plotted in Figs. 2(d)–2(f).

2. Squares—The case of two overlapping triads

For the case of two overlapping triads of wave vectors $\vec{k}_{n-m}=\vec{k}_n-\vec{k}_m,\vec{k}_m,\vec{k}_n$ and $\vec{k}_m,\vec{k}_n,\vec{k}_m+\vec{k}_n=\vec{k}_{m+n}$, as in Fig. 4(b), Eqs. (16) read

$$(l_m-l_n)(P-k^2_{n-m})A_{n-m}A^*_{n-m} + l_m(P-k^2_m)A_mA^*_m + (l_m+l_n)(P-k^2_{m+n})A_{m+n}A^*_{m+n} = 0, \tag{18a}$$

$$(l_n - l_m)(P - k_{n-m}^2)A_{n-m}A_{n-m}^* + l_n(P - k_n^2)A_nA_n^* + (l_m + l_n)(P - k_{m+n}^2)A_{m+n}A_{m+n}^* = 0, \tag{18b}$$

$$\sigma_{n-m}A_{n-m} + \tau_1 A_m^* A_n^* - \gamma A_{n-m}(S - A_{n-m}A_{n-m}^*) = 0, \tag{18c}$$

$$\sigma_m A_m + \tau_1 A_{n-m}^* A_n^* + \tau_2 A_n^* A_{m+n}^* - \gamma A_m(S - A_m A_m^*) = 0, \tag{18d}$$

$$\sigma_n A_n + \tau_1 A_{n-m}^* A_m^* + \tau_2 A_m^* A_{m+n}^* - \gamma A_n(S - A_n A_n^*) = 0, \tag{18e}$$

$$\sigma_{m+n}A_{m+n} + \tau_2 A_m^* A_n^* - \gamma A_{m+n}(S - A_{m+n}A_{m+n}^*) = 0, \tag{18f}$$

where $S=2(A_{n-m}A_{n-m}^*+A_mA_m^*+A_nA_n^*+A_{m+n}A_{m+n}^*)$. These equations have solutions such that $\vec{k}_m$ and $\vec{k}_n$ are orthogonal and of equal length [so that $\vec{k}_m=(\pm 1/\rho_n, 1/\rho_m)$, $\vec{k}_n=(\mp 1/\rho_m, 1/\rho_n)$] and the amplitudes $A_{n-m}=A_{m+n}<A_m=A_n$ are real valued. Indeed, for $k_m^2=k_n^2\doteq k^2$ and $\vec{k}_m\cdot\vec{k}_n=0$ (so that $k_{n-m}^2=k_{m+n}^2=2k^2$), $\sigma_m=\sigma_n$ and $\sigma_{n-m}=\sigma_{m+n}$. Equations (18c) and (18f) and Eqs. (18d) and (18e), respectively, then become identical if $A_m=A_n$ and $A_{n-m}=A_{m+n}$. Equations (18) reduce to

$$2(P - 2k^2)A_{m+n}^2 + (P - k^2)A_m^2 = 0, \tag{19a}$$

$$\sigma_m + 2\tau A_{m+n} - \gamma(S - A_m^2) = 0, \tag{19b}$$

$$\sigma_{m+n}A_{m+n} + \tau A_m^2 - \gamma A_{m+n}(S - A_{m+n}^2) = 0, \tag{19c}$$

where $S=4(A_m^2+A_{m+n}^2)$, $\sigma_m=-(k^2)^2+2Pk^2-1$, and $\sigma_{m+n}=-4(k^2)^2+4Pk^2-1$. Solve Eq. (19a) for

$$k^2 = P\frac{A_m^2 + 2A_{m+n}^2}{A_m^2 + 4A_{m+n}^2} \tag{20}$$

and rewrite Eqs. (19b) and (19c) as

$$A_m^2 = \frac{A_{m+n}}{3\gamma}(2\tau - 4\gamma A_{m+n}), \tag{21a}$$

$$16\gamma A_{m+n}^3 - (12\tau\gamma + 9\gamma^2)A_{m+n}^2 + [4Pk^2 - 8(k^2)^2 + 1 + 2\tau^2]A_{m+n} + \tau[-(k^2)^2 + 2Pk^2 - 1] = 0. \tag{21b}$$

Substituting Eqs. (20) and (21a) into Eq. (21b), we obtain a quintic polynomial equation in A_{m+n} which we may solve numerically. For example, if $P=1$, $\gamma=1$, and $\tau=2$, $A_{m+n}\simeq 0.237\,76$, $A_m\simeq 0.491\,57$, and $k\simeq 0.8708$.

Notice that

$$\frac{|l_n|}{|l_m|} = \frac{\rho_m}{\rho_n} = \frac{m}{n} \simeq \phi_-,$$

so that the rhombicity used to find this solution puts the wave vectors near the curves $(\pm\rho[(2\pi)^2/\sqrt{5}A], \frac{1}{\rho})$. As a connection to the result of Proposition 2 in Sec. II F, it is illustrative to consider Eq. (15a) for the choice of d. After dividing through by $2[(2\pi)^4/A^2]R^2$, Eq. (15a) set equal to zero becomes

$$[m(q - md) + n(p - nd)]A_mA_m^* + \{(n - m)[(p - q) - (n - m)d] + (m + n)[p + q + (m + n)d]\}A_{m+n}A_{m+n}^* = 0.$$

This equation holds if

$$d = \frac{qm + pn}{m^2 + n^2} \simeq \hat{d} = \frac{q + p\phi_+}{m + n\phi_+},$$

and we recognize the quantities

$$m(q - m\hat{d}) \simeq \pm\frac{1}{\sqrt{5}} \simeq -n(p - n\hat{d})$$

of Proposition 2.

Suppose that we determine an optimal value of k^2 as described above. For $\vec{k}_m=(\pm 1/\rho_n, 1/\rho_m)$, $\vec{k}_n=(\mp 1/\rho_m, 1/\rho_n)$, $k_m^2=k_n^2=k^2$ if $R^2=(m^2+n^2)/k^2$. The optimal configuration can be achieved only if $R=\sqrt{(m^2+n^2)/k^2}$. Discrete invariance for this case is expressed by the relation

$$R\phi_+ \simeq \sqrt{\frac{n^2 + (m+n)^2}{k^2}} \quad \text{if} \quad \frac{n}{m} \simeq \phi_+.$$

Example solutions for values of R in multiples of ϕ_+ are plotted in Figs. 2(a)–2(c).

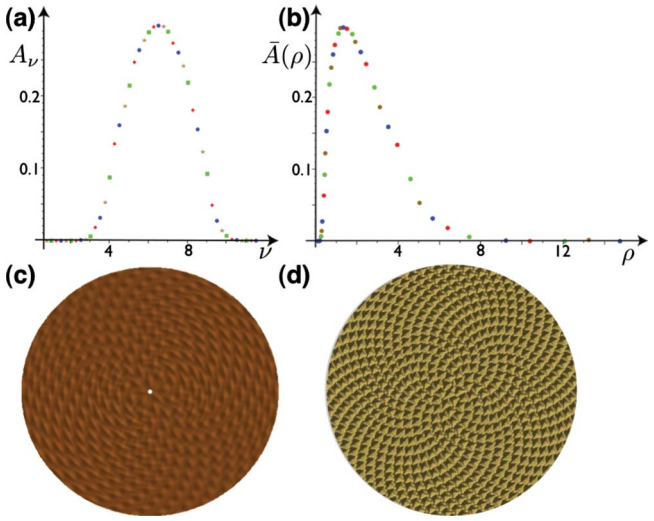

FIG. 5. (Color online) (a) Amplitudes $A(R/m_0\phi_+^{\nu+\mu})$, computed at $R_E=\sqrt{(13^2+21^2)/0.877^2}$ and $m_0=3$ as described in the text for $\mu=0$ (green squares), $\mu=\frac{1}{2}$ (blue dots), $\mu=\frac{1}{4}$ (brown asterisks), and $\mu=-\frac{1}{4}$ (red diamonds), (b) the amplitudes $\bar{A}(\rho)$ as a function of a $\rho=R_E/m_\nu$, (c) a graph of function (22), and (d) a graph of function (23).

3. *Offset squares—The case of three overlapping triads*

For the case of three overlapping triads $\vec{k}_{n-m}+\vec{k}_m-\vec{k}_n=0$, $\vec{k}_m+\vec{k}_n-\vec{k}_{m+n}=0$, and $\vec{k}_n+\vec{k}_{m+n}-\vec{k}_{m+2n}=0$, we obtain five equations from Eq. (16c). Similarly to the case of squares, Eqs. (16) have solutions for real-valued amplitudes $A_{n-m}=A_{m+2n}<A_m=A_{m+n}<A_n$ and wave vectors such that

$k_{n-m}^2=k_{m+n}^2$ and $k_m^2=k_{m+n}^2$, as depicted in Fig. 4(c). We call such solutions *offset squares* since they produce planforms of squares that do not meet at four-corner intersections [see Fig. 5(d)].

E. Continuous amplitude invariance

In Sec. III D 3, we have noted a discrete invariance as R changes in multiples of ϕ_+. The plant meristem size, as measured by R, often changes continuously with time. For example, in the sunflower floral meristem, the phyllotactic pattern starts at the outer edge of a disk and progresses inward to the center of the disk. In this case, R decreases. R increases as the shoot apical meristem of a seedling grows larger. In this section, we demonstrate how the pattern shifts between squares and offset squares as R changes continuously.

Consider again the square solutions with wave vectors $\vec{k}_{n-m},\vec{k}_m,\vec{k}_n=\vec{k}_{n-m}+\vec{k}_m$, $\vec{k}_{m+n}=\vec{k}_m+\vec{k}_n$ such that $k_m^2=k_n^2$, $k_{n-m}^2=k_{m+n}^2$, and associated real amplitudes $A_{n-m}\simeq A_{m+n}<A_m\simeq A_n$. These solutions may be generalized. Taking as our active set in Eqs. (13) any even set of $2n$ wave vectors $\vec{k}_{\nu-n+1},\vec{k}_{\nu-n+2},\ldots,\vec{k}_\nu$; $\vec{k}_{\nu+1},\vec{k}_{\nu+2},\ldots,\vec{k}_{\nu+n}$ in a Fibonacci-like sequence such that $\vec{k}_\nu^2=\vec{k}_{\nu+1}^2$ and $\vec{k}_\nu\cdot\vec{k}_{\nu+1}=0$ (so that $k_{\nu-k+1}^2=k_{\nu+k}^2$), we find solutions such that $A_{\nu-k+1}=A_{\nu+k}$ and such that the amplitudes decrease with decreasing k. A similar generalization may be made from the offset-square solutions to any odd set of wave vectors in a Fibonacci-like sequence.

Since the amplitudes $A_{\nu+k}$ of the modes decrease to zero as k increases, a square solution with only four modes may be a good approximation of a solution with a larger even number of modes, and an offset-square solution with only five modes may be a good approximation of a solution with a larger odd number of modes. We may make use of this to study the situation of increasing R. Consider a $\vec{k}_{\nu-n+1},\vec{k}_{\nu-n+2},\ldots,\vec{k}_\nu$; $\vec{k}_{\nu+1},\vec{k}_{\nu+2},\ldots,\vec{k}_{\nu+n}$. As calculated in Sec. III D, if a system has a preferred wave-vector length given by k^2, the square solution is realized at $R_1=\sqrt{(m_\nu^2+m_{\nu+1}^2)/k^2}$ as well as at $R_2=\sqrt{(m_{\nu+1}^2+m_{\nu+2}^2)/k^2}\simeq R_1\phi_+$. A function

$$\sum_{k=-n+1}^{n} A_{\nu+k}(R)\cos[\vec{k}_{\nu+k}(R)\cdot\vec{x}]$$

with the property that $A_{\nu+k}\to 0$ as k increases in magnitude thus has the property that

$$\sum_{k=-n+1}^{n} A_{\nu+k}(R_1)\cos[\vec{k}_{\nu+k}(R_1)\cdot\vec{x}]\simeq \sum_{k=-n+1}^{n} A_{\nu+k}(R_2 \simeq R_1\phi_+)\cos[\vec{k}_{\nu+k}(R_2\simeq R_1\phi_+)\cdot\vec{x}].$$

We now illustrate how we can capture the phyllotactic planform for continuously increasing R by making the ansatz that our solution is the sum of N modes with wave vectors in a Fibonacci-like sequence and allowing the amplitudes and wave vectors to change with R.

As a concrete example, we take as an ansatz that

$$w=\sum_{\nu=1}^{N=11} A_\nu e^{i\vec{k}_{m_\nu}\cdot\vec{x}}+\text{c.c.}$$

is a sum over $N=11$ modes with the Fibonacci-like sequence of wave vectors

$$\vec{k}_{m_0}=\vec{k}_3=\left(l_3,\frac{3}{R}\right),\quad \vec{k}_5=\left(l_5,\frac{5}{R}\right),$$

$$\vec{k}_8=\vec{k}_3+\vec{k}_5,\ \ldots,\vec{k}_{m_{11}}=\vec{k}_{377}=\vec{k}_{144}+\vec{k}_{233}.$$

We thus have 11 equations [Eqs. (16c)] for the amplitudes as well as the two equations [Eqs. (16a) and (16b)] which we solve for $l_m=l_{13}$ and $l_n=l_{21}$. Solving the system (numerically) at $R_E=\sqrt{(13^2+21^2)/k^2}$, where $k=0.877$, and using the parameters $P=1.2$, $\gamma/\tau^2=1/10$, we obtain a set of amplitudes such that

$$A_5(R_E)\simeq A_{55}(R_E)<A_8(R_E)\simeq A_{34}(R_E)<A_{13}(R_E)=A_{21}(R_E),$$

and the remaining amplitudes are close to 0.

In Fig. 5(a), we plot $A_\nu(R_E)$ as a function of ν in green dots. Now recall the relation of discrete invariance (14), that is,

$$A_{m_\nu}(R)=A\left(\frac{R}{m_\nu}\right)=A\left(\frac{R}{m_0\phi_+^\nu}\right).$$

For any real number μ,

$$A_{m_\nu}(R_E\phi_+^\mu)=A\left(\frac{R_E\phi_+^\mu}{m_\nu}\right)=A\left(\frac{R_E}{m_\nu\phi_+^{\nu+\mu}}\right).$$

The amplitude solutions for $R=R_E\phi_+^\mu$, $\nu=\frac{1}{2}$, are plotted at the points $\nu+\mu=\nu+\frac{1}{2}$ in Fig. 5(a). This solution corresponds to offset-square solutions with

$$A_{13}(R_E\phi_+^{1/2})=A_{89}(R_E\phi_+^{1/2})<A_{21}(R_E\phi_+^{1/2})=A_{55}(R_E\phi_+^{1/2})<A_{34}(R_E\phi_+^{1/2}).$$

Solutions for $\mu=\frac{1}{4}$ and $\mu=-\frac{1}{4}$ are also plotted in Fig. 5(a). The result is a discrete picture of a curve

$$A\left(\frac{R_E}{m_0\phi_+^\nu}\right)=A(\nu),$$

which we call in [24] the *primordial shape curve*. The solutions for l_m and l_n depend, in accordance with Eq. (9), linearly on R. [In this case, the area A is nearly constant. If the area changes with R (as is the case for larger values of γ/τ^2), then this linear relation will not hold.] To emphasize that the amplitudes depend only on the quantities $\rho_\nu=R/m_\nu$, we also plot in Fig. 5(b) the data in Fig. 5(a) as a function $\bar{A}$ of $\rho=R_E/m_0\phi_+^\nu$.

As a visualization of how the planform changes with R, we plot, in Fig. 5(c), the function

$$w(r,\theta)=\sum_{\nu=1}^{11}\bar{A}\left(\rho=\frac{r}{m_\nu}\right)\cos[\vec{k}_\nu\cdot(r,\theta)], \tag{22}$$

where in polar coordinates (r,θ), r represents R, $\bar{A}$ is a (cubic) interpolation of the points in Fig. 5(b), and $\vec{k}_\nu=(l_\nu,m_\nu/r)$.

As a final example, we present an analytic expression for an amplitude curve $\bar{A}(\rho)$ motivated by Proposition 2 in Sec. II rather than computation from amplitude equations. Referring to expression (9) for $\vec{k}_\nu$, consider the quantities

$$\frac{1}{k_\nu^2}=\frac{\rho_\nu^2}{B^2\delta_\nu^2\rho_\nu^4+1},$$

where $B^2=(2\pi)^2/A^2$ and recall that $\rho_\nu=m_\nu/R$, $\delta_\nu=(m_\nu/g)(q_\nu-m_\nu d)$. Evaluated at $d=\hat{d}(m_\nu,m_{\nu+1},q_\nu,q_{\nu+1})$, δ_ν^2 is, by Proposition 2, approximately $\frac{1}{5}$. Defining a function

$$\hat{A}(\rho)=\frac{\rho^2}{B^2\frac{1}{5}\rho^4+1},$$

we have that

$$\hat{A}(\rho_\nu)\simeq\frac{1}{k_\nu^2}.$$

The point is that the amplitude $\hat{A}(\rho_\nu)$ is equal for wave vectors of equal length, is larger for wave vectors of smaller length, and approaches 0 as wave-vector length goes to infinity. This is consistent with our square- and offset-square amplitude-equation solutions. We plot in Fig. 5(d) the function

$$w(r,\theta)=\sum_{\nu=1}^{11}\hat{A}\left(\rho=\frac{r}{m_\nu}\right)\cos[\vec{k}_\nu\cdot(r,\theta)] \tag{23}$$

for $B=1$ and wave-vector sequence

$$\vec{k}_\nu=\left(l_\nu=\frac{1}{2}\rho_\nu\delta_\nu\simeq\frac{1}{2}\rho_\nu(-1)^\nu/\sqrt{5},\frac{m_\nu}{r}\right),$$

where $m_0=3$ and $m_1=5$. As the radius changes, the (square) shape of the primordia is constant, although the spirals of square shift passed each other. This we call *continuous planform invariance*.

IV. DISCUSSION

In this paper, we have found discrete and continuous invariances in phyllotactic lattices and planforms as the radius parameter R or the van Iterson parameter Γ changes. The primordial shape curve for amplitudes of Fourier modes, derived from amplitude equations or based on the number-theoretical relation of Proposition 2, gives a constant shape of the primordia as the radius varies. One may now ask how the shape of the primordia depends on the form of the primordial shape curve and how these shapes correspond to the Voronoi tesselations often used in the analysis of phyllotactic patterns [7,15]. We will address these questions along with analysis of scanning electron microscopy (SEM) images of cactus meristems in [4].

The derivations in this paper have been motivated by consideration of the mature sunflower seed heads in Fig. 1. How much do the shapes of primodia change from the time they form at the meristem to the mature stage? Some SEM images of sunflower meristems do show diamond shapes or hexagonal patterns [29], and similar structures are also seen in cactus meristems. But, in many plants shapes evolve as they mature, and in particular diamonds on cacti can evolve into hexagons. The challenge is to integrate an understanding of the growth processes with the geometric descriptions of the observed patterns and their evolution.

The algorithm for producing Figs. 5(c) and 5(d) was to compute amplitudes with the radius R as a parameter. This approximates a process by which a phyllotactic planform propagates as a front with changing radius. In [27], we analyze this front propagation by the simulation of PDEs.

Although we have focused on invariance and noble divergence angles, other patterns are also observed in nature. Indeed, even rational values of d, such as the value $d=\frac{3}{8}$ whose lattice is pictured in Fig. 3, are common on many succulents. Rational values of d are also found in whorled patterns, such as in decussate phyllotaxis. In [39], we discuss from the viewpoint of PDE models how anisotropies in the physical parameters can favor rational divergence angles and transitions between patterns that display defects. Furthermore, as Williams [42] pointed out and as we discuss in the context of biochemical and biomechanical models in [25], various planform shapes are compatible with a given phyllotactic arrangement. These patterns, as well as related ridge-dominated planforms, will be analyzed in [4] using Voronoi tesselations with varying metrices and in comparison with data from cactus apices. Finally, we mention that global invariance is apparent in other natural systems, such as viral capsids [17].

ACKNOWLEDGMENTS

This work was supported by NSF Grant No. DMS-0503196 and benefited from collaboration and many discussions with Alan Newell and with Todd Cooke. The author also gratefully acknowledges Richard James for discussions that led to the results of Sec. II F, as well as the Max-Planck-Institute for Mathematics in the Sciences in Leipzig for hospitality in the summer of 2007.

[1] P. Atela, C. Golé, and S. Hotton, J. Nonlinear Sci. **12**, 641 (2002).
[2] I. Bravais and A. Bravias, Annales des Sciences Naturelles Botanique **7**, 42 (1837).
[3] A. H. Church, *On the Relation of Phyllotaxis to Mechanical Laws* (Williams and Norgate, London, 1904).
[4] T. J. Cooke and P. D. Shipman (unpublished).
[5] H. M. S. Coxeter, *Introduction to Geometry* (Wiley, New York, 1989).
[6] M. C. Cross and P. C. Hohenberg, Rev. Mod. Phys. **65**, 851 (1993).
[7] R. Dixon, *Symmetry in Plants*, edited by R. V. Jean and D. Barabé (World Scientific, Singapore, 1998), Chap. 13, pp. 213–333.
[8] S. Douady, *Symmetry in Plants*, edited by R. V. Jean and D. Barabé (World Scientific, Singapore, 1998), Chap. 14, pp. 335–358.
[9] S. Douady and Y. Couder, J. Theor. Biol. **178**, 255 (1996).
[10] S. Douady and Y. Couder, J. Theor. Biol. **178**, 275 (1996).
[11] C. Gollwitzer, I. Rehberg, and R. Richter, J. Phys.: Condens. Matter **18**, S2643 (2006).
[12] P. B. Green, Am. J. Bot. **86**, 1059 (1999).
[13] G. H. Hardy and E. M. Wright, *An Introduction to the Theory of Numbers*, 5th ed. (Clarendon, Oxford, 1979).
[14] S. Hotton, Ph.D. thesis, University of California–Santa Cruz, 1999.
[15] S. Hotton, V. Johnson, J. Wilbarger, K. Zwieniecki, P. Atela, C. Golé, and J. Dumais, J. Plant Growth Reg. **25**, 313 (2006).
[16] R. Hoyle, *Pattern Formation: An Introduction to Methods* (Cambridge University Press, Cambridge, 2006).
[17] R. D. James, J. Mech. Phys. Solids **54**, 2354 (2006).
[18] R. V. Jean, *Phyllotaxis: A Systematic Study in Plant Morphogenesis* (Cambridge University Press, Cambridge, 1994).
[19] *Symmetry in Plants*, edited by R. V. Jean and D. Barabé (World Scientific, Singapore, 1998).
[20] H. Jönsson, M. Heisler, B. E. Shapiro, E. M. Meyerowitz, and E. Mjolsness, Proc. Natl. Acad. Sci. U.S.A. **103**, 1633 (2006).
[21] W. J. Kelly and T. J. Cooke, Am. J. Bot. **90**, 1131 (2003).
[22] W. B. Krantz, K. J. Gleason, and N. Caine, Sci. Am. **259**, 68 (1988).
[23] A. C. Newell and P. D. Shipman, J. Stat. Phys. **121**, 937 (2005).
[24] A. C. Newell and P. D. Shipman, Analysis and Applications **6**, 383 (2008).
[25] A. C. Newell, P. D. Shipman, and Z. Sun, J. Theor. Biol. **251**, 421 (2008).
[26] A. C. Newell, P. D. Shipman, and Z. Sun, Plant Signal. Behav. **3**, 586 (2008).
[27] A. C. Newell, P. D. Shipman, and Z. Sun (unpublished).
[28] R. Occelli, Ph.D. thesis, University of Provence–Marseille, 1985.
[29] J. H. Palmer, *Symmetry in Plants*, edited by R. V. Jean and D. Barabé (World Scientific, Singapore, 1998), Chap. 7, pp. 145–169.
[30] D. Reinhardt, T. Mandel, and C. Kuhlemeier, Plant Cell **12**, 507 (2000).
[31] D. Reinhardt, E.-R. Pesce, P. Stieger, T. Mandel, K. Baltensperger, M. Bennett, J. Traas, J. Friml, and C. Kuhlemeier, Nature (London) **426**, 255 (2003).
[32] J. N. Ridley, Math. Biosci. **58**, 129 (1982).
[33] F. J. Richards, Philos. Trans. R. Soc. London, Ser. B **235**, 509 (1951).
[34] N. Rivier, R. Occelli, J. Pantaloni, and A. Lissowski, J. Phys. (Paris) **45**, 49 (1984).
[35] N. Rivier, J. Phys. (France) **47**, C3-299 (1986).
[36] H. Rivier, Mod. Phys. Lett. B **2**, 953 (1988).
[37] F. Rothen and A. J. Koch, J. Phys. (France) **50**, 633 (1989).
[38] P. D. Shipman and A. C. Newell, Phys. Rev. Lett. **92**, 168102 (2004).
[39] P. D. Shipman and A. C. Newell, J. Theor. Biol. **236**, 154 (2005).
[40] R.S. Smith, S. Guyomar'h, T. Mandel, D. Rheinhardt, C. Kuhlemeier, and P. Prusinkiewicz, Proc. Natl. Acad. Sci. U.S.A. **103**, 1301 (2006).
[41] G. van Iterson, *Mathematische und Mikroskopisch-Anatomische Studien ueber Blattstellungen* (Verlag von Gustav Fischer, Jena, 1907).
[42] R. F. Williams, *The Shoot Apex and Leaf Growth* (Cambridge University Press, Cambridge, 1975).